Michigan In-Space Servicing Orbiter: Concept Study of an In-Space Refueling and Resupply Depot

Devin Mroz, Tao Sevigny, Ayush Pujara, Jina Patel, Calvin Wong, Serabi Francis, Armita Marpu, Yuvraaj Pasumarthy, and Ethan Landt
University of Michigan, Ann Arbor, MI, USA, 48109

This paper presents the conceptual design of the Michigan In-Space Servicing Orbiter (MISO), as part of the 2025-26 COSMIC Capstone Challenge. MISO is an orbital depot designed to support the growing ISAM industry by providing propellant refueling and modular component transfer services to servicer spacecraft operating in Geostationary Earth Orbit (GEO). The depot is stationed in a sub-GEO orbit at 34,786 km, selected to minimize Δv requirements for visiting servicer spacecraft while maintaining a feasible response time. Six docking ports spanning five interface standards provide mechanical capture and fluid transfer capability. A closed-loop propellant architecture enables the storage and transfer of up to 7,000 kg of hydrazine, while a 7-DOF robotic manipulator facilitates the exchange of modular orbital replacement units from an internal cargo bay. Demand-driven resupply missions sustain the depot's inventories throughout a 15-year lifetime. The design is supported by detailed subsystem analyses including orbital mechanics trade studies, transient thermal modeling, radiation environment characterization, structural sizing, link budget analysis, and a full lifecycle cost and revenue model. Financial analysis projects a total lifecycle cost of ~$1.65 billion against lifetime revenue of $5.4 to $8.7 billion. The study demonstrates the technical and economic feasibility of a persistent depot architecture as foundational infrastructure for scalable ISAM operations.

I. Introduction

The space industry is undergoing a fundamental shift from single-use missions toward interconnected and sustainable space infrastructure. Historically, satellites have been designed as "one-and-done" systems launched with a fixed lifetime and discarded once fuel is depleted or components degrade. However, advances in in-space servicing, assembly, and manufacturing (ISAM) are enabling a new paradigm in which spacecraft can be refueled, repaired, upgraded, and assembled in space. As [1] describes, ISAM capabilities can vastly expand the performance, availability, and lifetime of space systems compared to the traditional paradigm of assets.

ISAM technologies have already demonstrated the ability to extend satellite lifetimes, reduce costs, and enable capabilities that would be constrained by launch vehicle limitations. Servicing missions can refuel and reposition satellites, while in-space assembly allows for the construction of large structures beyond fairing size constraints. Foundational demonstrations such as the ISS, Hubble Space Telescope servicing, and Northrop Grumman's Mission Extension Vehicle (MEV) have validated the operational potential of these capabilities [1]. The technologies are widely recognized as fundamental to the development of a sustainable and scalable space economy.

At the same time, the number of operational satellites is rapidly increasing. This growth is driving demand for logistics, maintenance, and life-extension services, creating a multi-billion-dollar market for on-orbit servicing solutions. As a result, both government agencies and commercial entities are investing heavily in ISAM technologies to support future exploration, national security, and commercial operations.

In response to these emerging needs, this paper presents the Michigan In-Space Servicing Orbiter (MISO) concept: an orbital platform designed to provide propellant storage and component logistics. By integrating refueling with component storage into a single platform, MISO aims to enable reusable mission architectures and reduce the cost and complexity of satellite operations. This paper provides a comprehensive overview of the concept, including its mission objectives, system architecture, business case, and supporting analyses. The discussion spans conceptual design, subsystem development, operational considerations, and economic feasibility, ultimately assessing the system's potential to contribute to a sustainable in-space logistics infrastructure.

II. Motivation and Mission Rationale

The traditional paradigm of spacecraft design, where satellites are fully integrated systems without means of maintenance, imposes significant limitations on both performance and economic efficiency. Satellite lifetimes are often constrained by consumables such as propellant and by component degradation from radiation. As a result, otherwise functional spacecraft with mostly working components are decommissioned, leading to inefficient use of resources.

In-space servicing offers a transformative solution to these challenges by enabling the extension, repair, and upgrade of existing assets. ISAM fosters an ecosystem that fundamentally changes the space operations paradigm, creating a foundation for sustainable exploration and serving as a force multiplier for capabilities such as space logistics, power generation, and reusability [1]. By refueling satellites and replacing critical components, servicing infrastructure can significantly increase mission lifetimes and improve return on investment for satellite operators.

From a commercial perspective, the rapid expansion of satellite constellations and high-value assets in Geostationary Earth Orbit (GEO) has created strong demand for servicing and logistics solutions. Existing demonstrations, such as MEV-1, have already proven the viability of servicing as a revenue-generating activity. However, current approaches are limited to single-purpose servicers, lacking the scalability and flexibility required for a mature servicing space economy.

The MISO concept is motivated by the need to transition from mission-specific servicing vehicles to persistent, multi-functional infrastructure. By acting as an orbital distribution hub, MISO reduces the operational burden on individual servicers and enables a more efficient logistics network. This shift mirrors the evolution of terrestrial transportation systems, where centralized depots and infrastructure dramatically improved scalability and cost efficiency.

III. Conceptual Mission Architecture

A. Overview

MISO is an autonomous orbital depot that provides propellant resupply and modular component transfer services to client spacecraft operating in the GEO regime to reduce per-mission costs and mass penalties. Standardized docking and servicing interfaces allow for multiple customers to access the depot for service. The depot is launched into an elliptical transfer orbit aboard a Falcon Heavy and uses its iodine-fed Hall-effect propulsion system to circularize to its operational altitude of 34,786 km over approximately three years.

The operational concept follows a fixed-orbit servicing paradigm: the depot remains stationed in its designated orbit while client spacecraft perform rendezvous, proximity operations, and docking (RPOD). In the near term, the primary clients are expected to be dedicated servicing spacecraft that act as intermediaries between the depot and legacy satellites lacking sufficient maneuvering capability, though future spacecraft with standardized servicing interfaces may access the depot directly. All visiting vehicles are assumed to carry compatible guidance, navigation, and control (GNC) systems and standardized docking interfaces for autonomous or supervised docking.

The depot's propellant refueling architecture is based on hydrazine, selected for its widespread use in GEO satellite propulsion systems, with a total storage capacity of 7,000 kg across seven bladder tanks. The initial deployment launches with a full propellant load to maximize initial revenue-generating inventory. In addition to propellant services, the depot provides modular resupply components stored within an internal cargo bay and transferred via an onboard robotic manipulator. Subsequent resupply missions, triggered by inventory depletion, leverage rideshare launch opportunities to restore the depot to full operational capacity.

B. Primary Mission Objectives

The MISO mission is structured around two primary demonstration objectives. The first is to demonstrate on-orbit propellant storage and transfer, validating the depot's ability to receive, store, and dispense hydrazine to docked client vehicles through a pressure-regulated fluid transfer system. The second is to demonstrate on-orbit component storage and transfer via a robotic arm, confirming the depot's capability to exchange orbital replacement units (ORUs) such as solar array modules, antenna assemblies, and battery packs. Mission success is demonstrated by completing mechanical docking with a visiting vehicle, executing propellant transfer operations within specified flow-rate and quantity margins or completing at least one robotic component handoff, and maintaining continuous telemetry throughout. Full mission success requires sufficient cumulative transfers to achieve profitability.

IV. Business Case Analysis

To assess the economic viability of the MISO concept, a comprehensive business case analysis was conducted, incorporating lifecycle cost estimation and a demand-driven revenue model based on projected GEO servicing adoption. Conservative assumptions were applied across development, manufacturing, launch, and operations to ensure robustness. The estimates were used to evaluate long-term profitability under both early-market and mature ISAM conditions.

A. Cost Estimate

The total lifecycle cost is estimated to be about $1.65B, including development, production, launch, and operation. Development costs include research and development (R&D), system design, and program management over an estimated five-year build period. Production costs account for manufacturing, integration, and testing. Launch costs are based on a Falcon Heavy-class vehicle.A development overhead allocation and a contingency margin of approximately 30% is applied to account for technical and programmatic uncertainties. The operations phase includes recurring costs such as mission operations, maintenance, insurance, and corporate administrative expenses over the depot's operational lifetime. Additionally, periodic resupply missions using rideshare, estimated at $45M to $110M per mission to GTO-class orbits, are incorporated as a recurring cost driver tied directly to servicing demand and propellant throughput.

Table 1 summarizes the estimated costs.

Table 1 MISO Lifecycle Cost Breakdown

Cost Category	Estimated Cost (USD)
Research & Development (R&D)	$180M
Manufacturing	$350M
Integration and Testing	$80M
Launch	$100M
Development Overhead	$120M
Contingency (30%)	$260M
Operations (Lifetime)	$380M
Insurance	$130M
Corporate/Admin	$50M
Total Lifecycle Cost	**$1.65B**

B. Revenue Model

The revenue model yields a projected lifetime revenue of $5.4B to $8.7B USD after incorporating revenue streams from fuel sales, membership-based services, component resupply, and on-orbit storage services. Pricing tiers are designed to incentivize long-term customer engagement. The diversified structure reduces reliance on any single revenue stream and improves resilience to market variability.

1. Fuel Revenue

The core revenue stream of hydrazine propellant sales is project to total $3.5B to $5.5B over the 15-year operational lifetime. Using Northrop Grumman's Mission Extension Vehicle (MEV) as a baseline client, the analysis assumes an average of 300 kg of fuel per transfer, with pricing structured across tiered memberships ($100k to $170k per kg depending on the tier). This results in an average revenue of approximately $30M to $40M per servicing mission. Annual fuel revenue scales with frequency of servicing operations, as seen in Table 2.

2. Membership Model

To stabilize revenue and incentivize long-term engagement, a membership model will be implemented which generates projected lifetime revenue of $1.5B to $2.2B. Two membership tiers are offered: Tier 1 (Premium) offers the largest price reductions, while Tier 2 (Standard) offers discounted pricing relative to the baseline. Both membership tiers provide reserved servicing slots and priority docking access. The membership structure is designed to benefit

Table 2 Annual Fuel Revenue

Phase	Operations per Year	Revenue
Early	3	$100M/year
Growth	8	$290M/year
Mature	15	$540M/year

servicers with moderate to high operational frequency. Specifically, for customers servicing at least four clients per year, the membership provides a net cost advantage relative to baseline pricing. This pricing strategy incentivizes repeat utilization of the depot while supporting long-term customer retention. A summary of the membership structure is provided in Table 3.

Table 3 Membership Model Structure

Revenue Stream	Description
Tier 1 Membership	Priority access + maximum discounts
Tier 2 Membership	Priority access + discounted pricing
Tier 3 (Baseline)	Standard pricing for fuel and components

3. Component Revenue and On-Orbit Storage Services

Additional revenue is generated through the sale of high-value spacecraft components, including batteries, solar arrays, and antenna systems. Demand is mission-driven and tied to servicing operations, with estimated lifetime revenue of $300M to $800M.

The depot also provides volumetric storage services priced per cubic meter per month. While initially a minor contributor, this revenue stream grows with ISAM market maturity, generating $50M to $200M over the system lifetime.

C. Business Outlook and Profitability

The financial model reflects a phased growth trajectory aligned with ISAM market adoption. Revenue during early years is constrained by capital expenditure and low servicing frequency (2 to 5 operations/year). As adoption increases, operation frequency scales to 6 to 10 operations/year during growth, and ultimately to 12 to 20 operations/year in a mature market, driven by increased GEO servicing demand. Th break-even point is expected to occur between Year 12 and 14, corresponding to 4 to 6 years after operational deployment, as recurring revenues begin to offset lifecycle costs.

Key drivers of profitability include servicing frequency, adoption of membership tiers, and utilization of onboard storage capacity. Importantly, the depot's refillable architecture and scalable servicing model enable continued revenue generation beyond initial propellant inventory, supporting long-term operational sustainability and positioning the system as critical infrastructure within the emerging ISAM economy. A summary of the projected financial performance is provided in Figure 1.

V. ConOps and Operating Sequence

This section describes the primary sequence of events during the mission, including launch, orbit insertion, rendezvous procedure during operation, and end-of-life.

A. Launch and Orbit Insertion

The depot is launched by a SpaceX Falcon Heavy rocket into an elliptical transfer orbit with perigee at 185 km and apogee at 34,786 km. This orbit is similar to a Geostationary Transfer Orbit (GTO), but its apogee is 1,000 km lower. The depot's mass of roughly 26,000 kg, with margin, is within the Falcon Heavy's maximum payload mass to GTO of 26,700 kg, and its structure is designed to fit within the payload fairing.

After being placed into the transfer orbit, the depot fires its Hall Effect thrusters for roughly 3 years until the orbit is circularized to the operating altitude of approximately 34,786 km. Details on how the transfer time was calculated are

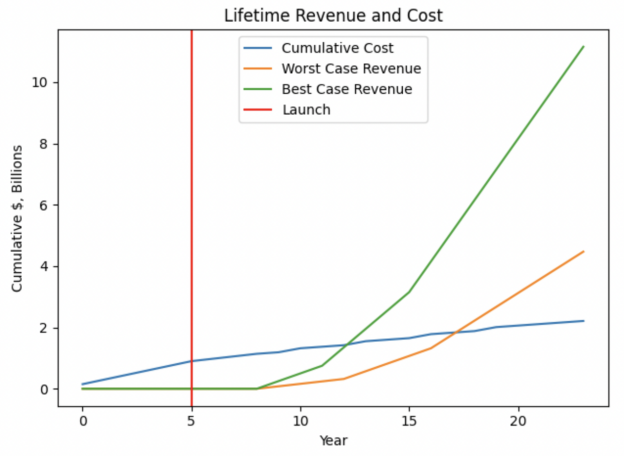

Fig. 1 This graph shows cumulative cost and revenue over the mission lifecycle, highlighting how profitability depends on market adoption rate.

provided in Section VIII C, Electric Propulsion Subsystem.

B. Depot Altitude Selection

The depot operates in a circular orbit with 0° inclination at an altitude of roughly 34,786 km, 1,000 km below GEO. After considering various options, this altitude was selected because it minimizes required Δv for servicers while maintaining a reasonable average response time, where response time is defined as the time it takes for a servicer to travel to the depot from its current position in GEO. The initial goal when selecting an altitude was to minimize response time. This was motivated by prospect of providing rapid support to a servicer that needs urgent repair. An optimization analysis showed that placing the depot at an altitude of 18,400 km would achieve a 90th percentile response time of 24 hours [2]. However, this created an unreasonable Δv requirement for servicers of 1.5 km/s [2]. Upon further analysis, the priority was shifted to minimizing the Δv requirement for servicers while maintaining a reasonable response time. This led to two primary options: placing the depot in GEO and placing it below GEO. Evaluating these options showed that while placing it in GEO gives more flexibility to servicers to choose their balance between Δv and response time, while placing it slightly below GEO requires less Δv on average.

The main benefit to servicers of a depot in GEO would be the flexibility to choose their balance between Δv and response time. With both satellites in the same orbit, Δv and response time are driven by the initial angular separation between the servicer and depot. The trade-off between the variables can be seen in Fig. 2. For any given angular separation, a servicer can either spend more Δv to minimize the response time by covering the entire separation angle with a limited number of phasing orbits, or it can minimize Δv by using more phasing orbits to gradually cover the separation angle. For example, assume the servicer starts 90° ahead of the depot. It can close this separation in just over three days by entering a phasing orbit which closes 30° of separation with each orbit. This would require 158 m/s of Δv. Alternatively, it can spend 17 m/s to use a phasing orbit which would close 3° of separation with each orbit, resulting in a transfer time of 30 days. This concept would provide valuable flexibility to servicers to choose their transfer orbit based on their priorities.

However, placing the depot just below GEO will exchange this flexibility for a significant reduction in required Δv. In this case, the response time is dominated by the time a servicer has to wait for the right alignment to start a Hohmann Transfer. The Δv is set for any chosen depot altitude, but response time depends on initial angular separation, since that determines the wait time required for alignment. Fig. 3 shows how response time scales with depot altitude, where response time is averaged across all initial separation angles. The result is that for a comparable response time to the previous case, Δv tends to be lower. For example, a depot altitude of 1,000 km below GEO requires an average response time of 14 days and a Δv of just 19 m/s. This combination of response time and Δv could not be achieved if the depot were in GEO. Since the priority is minimum Δv, it is acceptable to sacrifice the option of ultra-low response times in favor of consistently lower Δv cost.

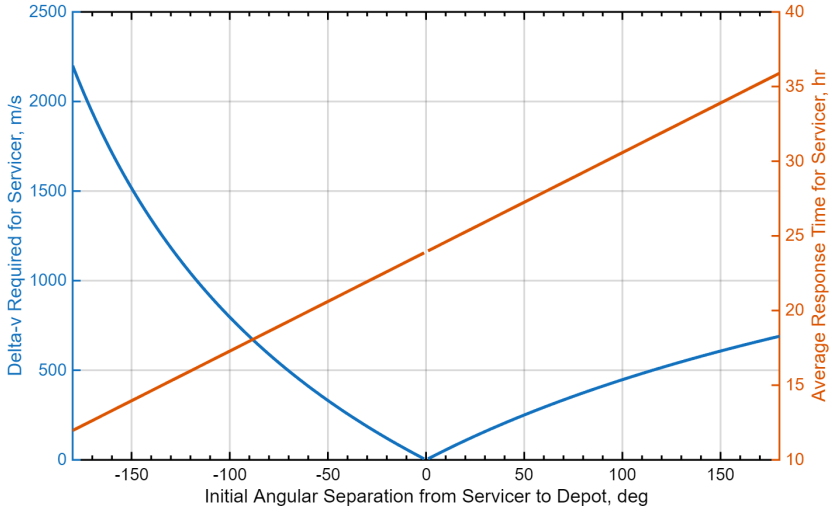

Fig. 2 For the case of the depot in GEO, Δv and response time vary with initial angular separation from the servicer to the depot. Positive angles lead to a phasing orbit with period >24 hours, and negative angles lead to one with period <24 hours.

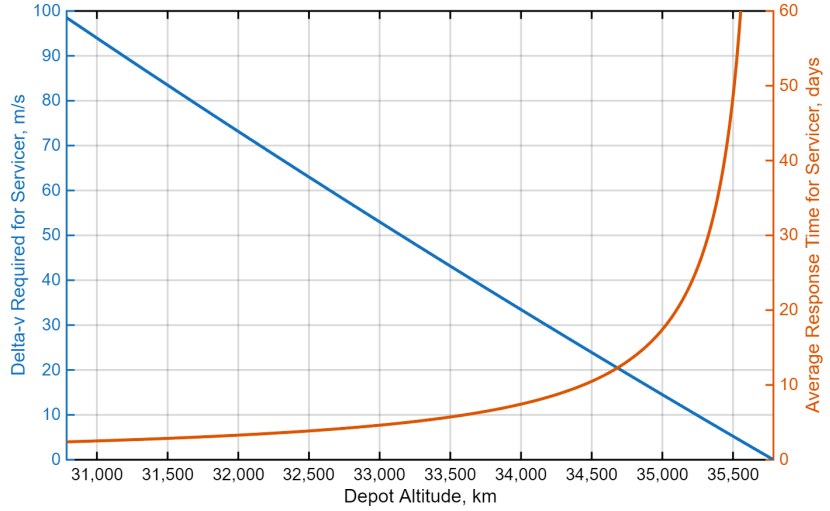

Fig. 3 For the case of the depot below GEO, Δv decreases linearly with altitude, while average response time begins to sharply increase between 34,000 and 35,000 km. Note that the average response time is in units of days.

C. Station-keeping

If left uncorrected, the depot's inclination would increase by about 1° per year, so the depot will use its thrusters to correct this inclination drift with North-South station-keeping maneuvers. The RAAN of the orbit will also drift over time, but since there are no other satellites currently at that altitude which pose a collision risk, there is no need to correct the RAAN drift.

D. Near-Field Rendezvous

Once a servicer is at close range to the depot, defined as within 10 km, it will perform its near-field rendezvous in a safe and controlled manner using a walking safety ellipse. Once it gets within 1 km of the depot, it will perform two burns to reduce the diameter of the ellipse. At that point, the servicer will switch to maneuvering using relative

navigation. The depot will have a set of AprilTags, the fiducation preferred by NASA's Exploration and In-space Services (NExIS) Projects Division, on all sides [3].

E. End-of-Life

When the depot reaches the end of its life and is no longer operational, it will be raised into the standard graveyard orbit for GEO satellites about 300 km above GEO. This will require roughly 47 m/s of Δv.

VI. System Requirements and Architecture

A. System Requirements

The system requirements for MISO were developed through a structured requirement flowdown process, beginning with high-level mission objectives. This approach ensures traceability between mission goals and subsystem design. Requirements are organized into two primary levels: top-level mission requirements (Level 1), which define overarching system objectives and capabilities; and system functional and performance requirements (Level 2), which specify the quantitative and qualitative criteria necessary to achieve mission success.

1. Top-Level Mission Requirements

The top-level mission requirements establish the fundamental objectives of MISO, emphasizing persistent operation, modular servicing capability, and operational autonomy. These requirements define the system as a reusable on-orbit infrastructure element capable of supporting a range of in-space servicing activities. A summary of the primary mission requirements is provided in Table 4.

Table 4 Top-Level Mission Requirements (Level 1)

Requirement ID	Description
L1-M-03	The spacecraft shall be capable of completing servicing operations in orbit without reliance on human involvement.
L1-M-04	The spacecraft shall be capable of transferring liquid propellant to a client satellite.
L1-M-05	The spacecraft shall be capable of transferring replacement components to a client spacecraft.
L1-M-08	The spacecraft shall be capable of being refuled by resupply spacecraft.
L1-M-11	The spacecraft shall be capable of reaching and operating within 1,000 km of GEO, including consideration for all environmental factors.

2. System Functional and Performance Requirements

System-level requirements define the functional capabilities and performance metrics required to satisfy the mission objectives. These requirements are allocated across major subsystems, including structures, propulsion, power, communications, GNC, thermal management, and servicing systems. Key requirements address propellant storage and transfer performance, robotic arm capability, docking interface compatibility, power generation and storage capacity, communication bandwidth, and system reliability over the 15-year design life. Environmental considerations, including radiation tolerance and thermal cycling near GEO, are also incorporated into subsystem requirements. A subset of representative system-level requirements is provided in Table 5.

B. System Architecture

The MISO system architecture is organized into three functional layers: mission management, which handles high-level planning, client communication, and safety monitoring; service management, which governs docking, proximity operations, and servicing execution; and resource management, which oversees propellant inventory, power distribution, thermal regulation, and system health. These layers are designed to support both autonomous and ground-supervised operations. Table 6 summarizes the primary architectural functions and their associated responsibilities.

Table 5 Representative System Functional and Performance Requirements (Level 2)

Requirement ID	Description
L2-STRC-01	The structure shall be designed to withstand all mechanical loads with a 1.4 safety factor.
L2-STRC-02	The system shall have a standard interface for client spacecraft to dock to.
L2-PROP-01	The propulsion system shall be able to insert the depot into its final orbit and maintain the orbit.
L2-REG-01	The system shall comply with strategies and regulations for debris mitigation and end-of-life.
L2-RA-02	The robotic arm subsystem shall support component transfer operations and shall not be required to perform docking or capture of a client servicer.

Table 6 Key System Architectural Functions

Function	Description
Mission Management and Safety	Controls overall mission flow, including communication, service request assessment, mission mode selection (planned vs. emergency), and safety/fault monitoring.
Guidance, Navigation, and Control (GNC)	Enables rendezvous with the client satellite through orbital state estimation, trajectory planning, path execution, proximity operations, and station-keeping.
Visiting Vehicle Interaction Management	Monitors and regulates approaching vehicles by defining keep-out zones, assigning docking ports, coordinating approaches, and enforcing proximity safety constraints.
Identification and Interface Verification	Ensures compatibility and correctness by identifying the target, verifying ICD compliance, recognizing visual markers, and validating docking geometry and authorization.
Capture, Anchoring and Stabilization	Manages physical interaction using a robotic arm to establish contact, dampen relative motion, engage anchoring mechanisms, and stabilize structural loads.
Resource Storage and Management	Maintains servicing resources, including fuel storage (monitoring, selection, routing) and module/parts inventory (tracking, preparation for transfer).
Servicing Operations	Executes core mission tasks such as satellite health assessment, module/part transfer, refueling, repair/replacement, and service verification.
Separation and Post-Service Operations	Handles safe mission closure through anchor release, controlled undocking, departure trajectory planning, and post-service clearance monitoring.
Station-keeping and System Support	Provides continuous background support including power/thermal management, robotics health monitoring, port readiness, fault detection/recovery, and ground override.

VII. Physical System Design

This section presents the physical system design of the depot, which includes the arrangement of subsystems, propellant storage, payload accommodation, and external interfaces. The design of the depot ensures compatibility with launch vehicle constraints, efficient volume utilization, and the ability to support on-orbit servicing operations.

A. Spacecraft Configuration

The depot satellite is designed as a hexagonal prism, as shown in Figure 4a, to support in-orbit refueling and payload transfer. The primary structure consists of six aluminum corner beams connected by honeycomb sandwich panels, forming the side walls, base plate, mid plate, and top plate. This hexagonal prism bus allows for internal storage of payloads, fuel, and subsystems, shown in Figure 4b, as well as six accessible ports for client satellites to dock to the depot.

B. Layout

The internal layout is organized to separate payload handling and propellant storage while maintaining a balanced center of mass and efficient system integration. The spacecraft is divided into two primary sections: the payload bay (upper section) and the fuel bay (lower section), as shown in Figure 5. The payload bay houses client-deliverable hardware, including 3 deployable antennas, 30 batteries, and 4 roll-out solar arrays. The fuel bay contains all propellant

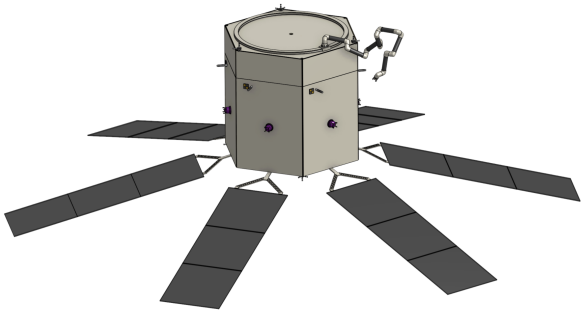

(a) Hexagonal depot spacecraft with deployed solar arrays and robotic arm.

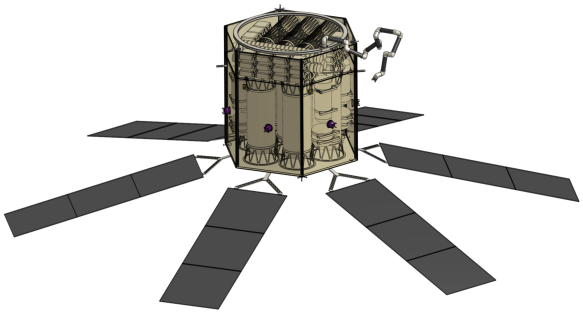

(b) Internal component arrangement and primary load-bearing frame.

Fig. 4 CAD images of depot spacecraft.

storage and plumbing, including 7 hydrazine tanks for client refueling, 4 iodine tanks for electric propulsion maneuvers, and 4 helium tanks for pressurization. The propellant tanks are arranged symmetrically around the spacecraft centerline to minimize center of mass offsets, ensuring stable attitude control. Externally, the spacecraft features six docking interfaces (one per side panel), a 7-DOF robotic arm mounted on a 360º rail, six deployable solar arrays, antennas for ground and client communications, and RCS cold gas thrusters for attitude control. This layout allows for parallel servicing operations and robotic accessibility to all docking ports.

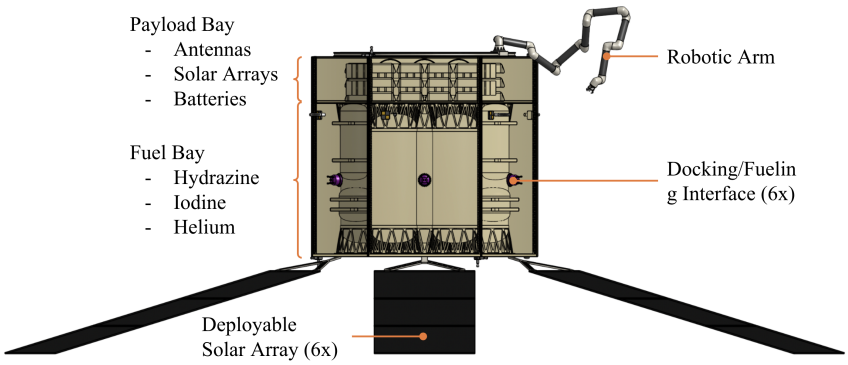

Fig. 5 General layout of depot.

C. Dimensions and Volume Constraints

The spacecraft dimensions are driven by the launch vehicle constraints, propellant/payload storage requirements, and power generation needs. Figure 6a shows the general dimensions of the depot. With the robotic arm and solar arrays stowed, the depot has a height of 3.57 m and a width of 3.51 m. In this stowed configuration, the footprint of the depot fits within SpaceX's Falcon Heavy payload fairing, shown in Figure 6b. When the depot's solar arrays are fully deployed, it will have a full span of 16.26 m. The depot is designed to maximize usable internal volume to store the payload, fuel, and subsystems while remaining within launch vehicle constraints.

VIII. Key Subsystems

The MISO platform has various key subsystems that define the technical foundation of the architecture. First, the Client Refueling subsystem enables standardized, reliable propellant transfer to a range of servicing clients. The Component Transfer subsystem, consisting of a modular cargo bay and robotic manipulation system, supports the delivery, exchange, and installation of critical hardware elements. The Electric Propulsion subsystem provides high-efficiency

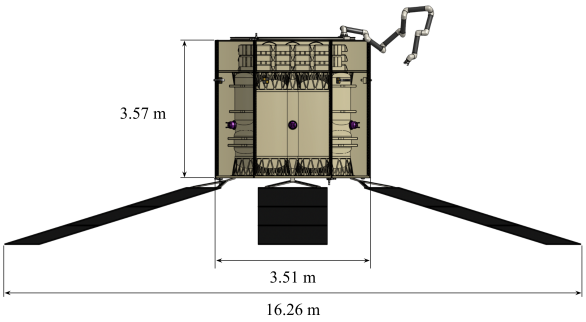

(a) Spacecraft dimensions in deployed configuration.

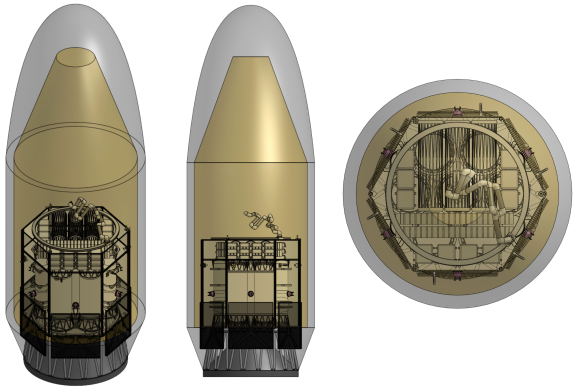

(b) Spacecraft stowed configuration within Falcon Heavy payload fairing envelope.

Fig. 6 Spacecraft in deployed and stowed configurations.

orbital insertion and station-keeping capability. Finally, the Communications subsystem ensures robust command, telemetry, and high-rate data transfer, maintaining continuous situational awareness and operational control.

A. Client Refueling Subsystem

The client refueling subsystem provides the depot's core propellant transfer capability, storing and dispensing hydrazine to visiting spacecraft through a regulated, pressure-fed architecture designed to support sequential refueling operations over the depot's 15-year mission life.

Hydrazine is stored in seven titanium bladder tanks (Ti-6Al-4V) that each have a volume of approximately 1,000 L, providing a total propellant storage capability of 7,000 kg. Bladder construction ensures positive expulsion in microgravity by maintaining a physical barrier between pressurant gas and liquid propellant. Each tank is wrapped in multi-layer insulation and equipped with active heaters to maintain propellant within the 10 to 40°C operational band. Screen-channel and vane-type capillary propellant management devices direct liquid toward the tank outlet during transfer operations. The tanks are interconnected through a cross-feed ring that balances propellant levels to maintain the depot's center of mass within attitude control authority and enables any tank to feed any outlet port.

Pressurization is provided by a regulated helium system comprising four composite overwrapped pressure vessels (COPVs) with titanium liners and carbon fiber/epoxy overwrap, each sized at approximately 230 L and carrying a total of roughly 40 kg of helium. Unlike conventional open-loop architectures, the pressurant system employs a closed-loop recovery design that enables helium reuse across multiple refueling cycles. During propellant transfer to a client vehicle, regulated helium is introduced into the gas side of the selected hydrazine tank to maintain expulsion pressure. During depot refill operations, incoming hydrazine displaces ullage helium, which is recovered through a return manifold, filtered to remove entrained contaminants, collected in a low-pressure accumulator, and recompressed for return to the COPVs. This closed-loop architecture turns helium into a recyclable working fluid, significantly reducing lifetime pressurant mass requirements.

The refueling manifold incorporates redundant safeguards including dual isolation valves at each tank outlet and interface port; burst disks for overpressure protection; inline pressure, temperature, and flow instrumentation for real-time transfer monitoring; and vent and purge lines for inter-operation line evacuation and integrity verification.

A weighted trade study evaluated seven candidate docking and refueling interfaces against four mandatory criteria (mechanical docking capability, fluid transfer support, U.S. manufacture, and TRL above 4) and fourteen performance metrics including structural load capacity, alignment tolerance, flight heritage, and cost. A multi-interface configuration scored highest by maximizing the number of compatible clients at the cost of added integration complexity. The resulting baseline comprises two OrbitFab RAFTI ports, one Northrop Grumman PRM, one SpaceWorks FuseBlox, one iBOSS iSSI, and one Enduralock OneLink, yielding six docking and refueling ports spanning the broadest commercially available interface ecosystem.

Prior to initiating propellant flow, the fluid connection is verified through a visual leak check using the robotic arm's onboard camera. Once a leak-free connection is confirmed, pressurized hydrazine is driven through the manifold and

into the client's tanks. Transfer is terminated upon reaching the target delivery quantity or upon detection of a pressure, temperature, or flow anomaly. Lines are then purged and disconnected before the client vehicle departs.

B. Component Transfer Subsystem

The component transfer subsystem enables the depot to store, manage, and exchange ORUs with docked client spacecraft. This capability complements refueling by allowing clients to receive hardware upgrades or replacement modules without having a dedicated servicing vehicle, consolidating both functions into a single platform.

1. Cargo Bay and Components

The cargo bay is organized into two storage configurations selected based on component types with the highest projected demand for on-orbit repair and augmentation. A long-item canister lane accommodates elongated payloads, specifically solar array replacement kits and antenna module canisters. A dense-mass pallet rack provides structured storage for compact, high-mass items such as battery ORUs. The baseline component manifest includes three categories of hardware. Solar array kits, based on the ROSA-class roll-out wing form factor, have a stowed width of 2.7 m and a stowed volume of approximately 0.13 m^3 at a mass of 43 kg per unit. Antenna replacement kits, sized to the unfurlable mesh reflector canister class, measure 2.1 m in height and 0.55 m in diameter at a mass of 54 kg. Battery replacement modules, representative of standard energy storage ORUs, measure 0.44 m in height and 0.39 m in diameter with a volume of 0.03 m^3 and a mass of 29 kg per unit. These dimensions and masses were derived from a survey of representative GEO satellite servicing hardware and scaled to be compatible with the depot's structural envelope and robotic arm payload capacity.

2. Robotic Arm

A system-level trade study was conducted to establish the baseline architecture for the robotic arm, with emphasis on high-load stability and payload safety. Three configurations were evaluated: a rigid arm with a soft end effector, a soft arm with a rigid end effector, and a fully rigid commercial off-the-shelf (COTS) arm. A configuration with a rigid arm paired with a soft end effector provided the best overall performance. Carbon fiber-reinforced polymer (CFRP) for the rigid arm segments provides high structural stiffness due to its high stiffness-to-weight ratio. This makes the arm capable of handing payloads exceeding 55 kg at full extension while maintaining precise positioning and avoiding the low-frequency oscillations associated with fully soft arms using brushless DC motors at each joint. Simultaneously, the soft end effector conforms to the payload surface using a foldable Kresling origami structure. The mechanism is constructed from space-grade aluminum panels connected by Kapton tape hinges, allowing conformity to a range of component geometries while distributing contact forces. This approach reduces the risk of damaging sensitive hardware while avoiding long-term degradation and outgassing concerns associated with conventional soft polymer robotics. This hybrid architecture enables reliable load transfer and safe handling of components.

Component transfer operations are performed using a 7-DOF custom rigid manipulator with a total reach of 4.55 m. The arm consists of seven 0.65 m segments which were determined through forward and inverse kinematic models using nominal and worst-case target locations within the 3 m × 2 m × 1.5 m servicer workspace. The seventh degree of freedom introduces kinematic redundancy, allowing the arm to avoid singularities and maneuver around structural constraints within the depot. This redundancy proved particularly valuable in confined scenarios. For example, the inverse kinematics solver required 213 iterations to converge for a worst-case corner target, compared to 33 iterations for a direct reach. Despite this variation, the system consistently achieved end-effector positioning errors of ∼0.9 mm across all simulated trajectories. Based on these results, a minimum reach of 4.3 m was required. Incorporating a 5% safety margin increased this to 4.52 m, which is satisfied by the final 4.55 m design.

To support safe and reliable operation in a vacuum, the system incorporates sensing across three categories: end-effector exteroception, joint proprioception, and structural health monitoring. The end effector is equipped with a suite of sensors designed to support target acquisition, approach guidance, and safe contact during component handling. Two co-linearly paired space-grade stereo vision cameras provide macro-targeting and depth perception at ranges from 1 to 10 m, identifying fiducial markers on components with the aid of two LED illuminators. A time-of-flight LiDAR unit supplements the cameras with millimeter-accurate range measurements, ensuring reliable distance data independent of lighting conditions. For the final 10 cm of approach, three short-range proximity micro-lasers detect when a component has crossed the capture threshold, triggering the grasp sequence. Contact safety is managed by a 6-axis force/torque sensor mounted at the wrist, which monitors forces in all three translational axes to prevent structural overloading during

transfer operations. Additionally, three thin-film tactile slip sensors, one per gripper, provide micro-haptic feedback by detecting shear forces at the contact surface, enabling the flight computer to adjust grip strength in real time without over-compressing hardware.

Each of the manipulator's seven joints is instrumented with dual absolute and incremental rotary encoders, totaling 14 units, which measure motor shaft rotation to ensure the arm halts at the commanded angle. Joint torque sensors integrated directly into the gearbox of each joint detect torque spikes indicative of unexpected contact, enabling the arm to stop immediately and prevent collisions with the client spacecraft or depot structures. Thermal monitoring is provided by seven thermistors, one per joint motor, which track motor temperatures during operation. Because heat dissipation in a vacuum is limited to radiation alone, these sensors allow the flight computer to pause operations and the arm to cool if motor temperatures approach thresholds.

Long-term structural integrity of the arm segments is monitored through three complementary sensing systems. Four thin-film resistance temperature detectors per segment map the thermal gradient along each link, enabling autonomous rotation of the arm to equalize solar exposure across the carbon fiber structure if localized temperature extremes are detected. Four fiber Bragg grating optical sensor strips per segment, bonded lengthwise along the top, bottom, left, and right faces of each tube, measure microscopic strain by detecting wavelength shifts in light transmitted through embedded fiber-optic cables, providing continuous monitoring of bending and axial loads. Finally, two acoustic emission sensors per segment detect the high-frequency stress waves generated by micrometeoroid impacts, allowing the ground team to localize impact sites along the arm and assess structural degradation before it progresses to a failure condition.

3. Component Transfer Operations

During a transfer operation, the cargo bay door is opened and the arm acquires the designated ORU from its storage slot. The arm then maneuvers the component to the client's installation interface, applies the necessary force to engage the mechanical connection, and verifies correct installation through both telemetry feedback and visual inspection using the arm-mounted camera. If the installation check fails, the arm disengages the component and resets for a re-attempt. Upon successful verification, the arm returns to its stowed configuration and the cargo bay is secured.

C. Electric Propulsion Subsystem

The depot's orbit-raising, station-keeping, and end-of-life disposal maneuvers are performed by a high-efficiency electric propulsion system, with chemical propellant reserved exclusively for client servicing. Chemical propulsion was ruled out for primary spacecraft maneuvering due to prohibitive propellant mass requirements at the depot's system mass.

A trade study evaluated five candidate propellants (xenon, iodine, krypton, argon, and hydrazine) against system-level criteria including volumetric efficiency, cost, GEO heritage, contamination risk, propulsion performance, and technology readiness level. Xenon, the current industry standard for Hall-effect systems, was penalized for its high cost and need for high-pressure storage, which increases tank mass and structural complexity. Krypton and argon were disadvantaged by lower thrust efficiency and poor volumetric density, while hydrazine was excluded due to its significantly lower specific impulse. Iodine scored highest, driven by its solid-phase storage at high density, elimination of high-pressure tankage, and substantial reductions in overall system mass. Although iodine introduces material compatibility and contamination challenges, these are mitigated through corrosion-resistant materials and established thermal control strategies, and recent in-orbit demonstrations support its growing maturity for electric propulsion applications.

An iodine-based Hall-effect thruster generates thrust by thermally sublimating solid iodine propellant at 120 to 140 °C to produce a gaseous feed, which is ionized in a discharge chamber and accelerated through a magnetized channel by an applied electric field [4]. A downstream neutralizer maintains charge neutrality and prevents spacecraft charging [4].

The depot employs eight Busek BHT-6000 Hall-effect thrusters, selected for their high thrust-to-power ratio and iodine compatibility. Eight engines are required because the total impulse for orbit raising was calculated at 58.9 MN·s, while each engine provides 8.5 MN·s [5]. This allocation covers orbit raising, station-keeping, end-of-life maneuvers, and margin. Only two engines operate simultaneously; powering additional engines would require a proportional increase in solar array area that was deemed infeasible within the depot's structural and mass constraints.

With two engines firing at full power in high-thrust mode (5,000 W, 325 mN, 2,000 s specific impulse per engine), the orbit-raising transfer from GTO to the operational altitude requires approximately 3 years. This estimate was derived by extrapolating results from Dankanich et al. [6], which present transfer time and Δv as functions of specific power and force-to-power ratio for a spacecraft mass of 19,000 kg. The corresponding Δv is approximately 3.0 km/s, requiring roughly 1,800 kg of iodine propellant.

D. Communications Subsystem

The MISO communications subsystem is designed to provide robust, secure, and flexible links for all phases of the mission, supporting telemetry, tracking, command (TT&C), high-rate data transfer, and proximity operations. The architecture integrates Earth-pointed links, short-range crosslinks, and an internal digital network, all centered on the command and data handling (C&DH) system, following standard system engineering principles outlined in [7].

1. Earth-Link Communications

Earth-link communications employ redundant S-band transceivers for TT&C, ensuring continuous spacecraft control even under off-nominal conditions. High-rate X-band downlink is utilized for imagery and video, routed through a high-gain antenna when Earth-pointed. All signals are encrypted to maintain secure operations.

The hardware suite includes: 2 S-band transceivers and 1 X-band high-rate transmitter; 2 S-band power amplifiers and 1 X-band high-power amplifier; 6 omni-directional antennas to maintain continuous coverage regardless of spacecraft orientation; 1 high-gain antenna for efficient high-rate data downlink; 1 RF switch matrix, low-noise amplifiers, and diplexers to separate signals by frequency; and integrated crypto engine for data encryption.

The X-band link was selected over Ka-band due to its capability to support 10 to 50 Mbps data rates, sufficient for 4k stills and short video clips, while offering robust performance under varying conditions, reduced pointing and thermal burden, and mature, low-risk technology.

Primary ground segment support is provided by KSAT, utilizing their 11.3 m and 13 m antennas. This upgrade from the originally planned 7 m class antenna provides approximately 4.1 dB additional gain, doubling the design margin to 8.6 dB, mitigating slant range and atmospheric attenuation risks, and enabling high-fidelity delivery of video and imagery. KSAT's polar station footprint further extends contact windows for a near-GEO orbit.

2. Proximity Crosslink

For close-range operations (< 10 km), MISO employs a dedicated proximity crosslink to enable low-latency, secure communication between the depot and visiting spacecraft. This link supports autonomous docking, propellant transfer, and component handoff operations.

Key attributes of the proximity crosslink include: short-range operation with latency under 1 s; redundant crosslink radios (2 units) with 6 patch antennas; authentication and encryption firmware for secure communications; and short-range power amplifiers optimized for energy efficiency and reliability.

3. Internal Digital Network

All communication flows are managed by a centralized C&DH system, which maintains a packetized telemetry network to enable real-time fault detection, mode management, and autonomous operations. The internal network includes a flight computer, solid-state recorder, SpaceWire router, high-altitude GNSS receiver (~ 10 W), watchdog hardware, and power conditioning units, providing a backbone for onboard decision-making and subsystem coordination.

4. Design Justification and Performance

This layered communication architecture provides continuous TT&C, high-rate data downlink, and short-range operational support while maintaining redundancy and encryption across all channels. By combining Earth-link, proximity crosslink, and internal digital networking, the subsystem ensures high reliability, low latency, and flexible support for all phases, consistent with the requirements for autonomous servicing and modular component transfer.

IX. System Budgets

A. Mass Budget

The mass budget was developed with a top-down, mission-constrained philosophy centered on maximizing on-orbit capability with our initial launch. The design is intentionally mass-limited to enable launch aboard a Falcon Heavy to GTO, which constrains the maximum payload capacity to ~26,700 kg. This constraint directly informed subsystem allocations, contingency margins, and propellant loading decisions.

A key driver of the mass budget is the inclusion of 7,000 kg of hydrazine. All of the categories are derived from component datasheet masses and CAD-based estimates. A summary of the mass distribution by category is provided

in Table 7. Note that the Propulsion category consists of the client refueling subsystem and the electric propulsion subsystem. A breakdown of this is shown in Figure!7.

Table 7 Mass Budget Summary by Subsystem

Category	Mass (kg)
Component Transfer & Interfaces	258
Structures	1,972
ADCS	235
Propulsion	17,455
Power	758
Communications & Avionics	48
Thermal	52
Dry Mass + Propellant	20,726
Total (with 25% Margin)	25,908

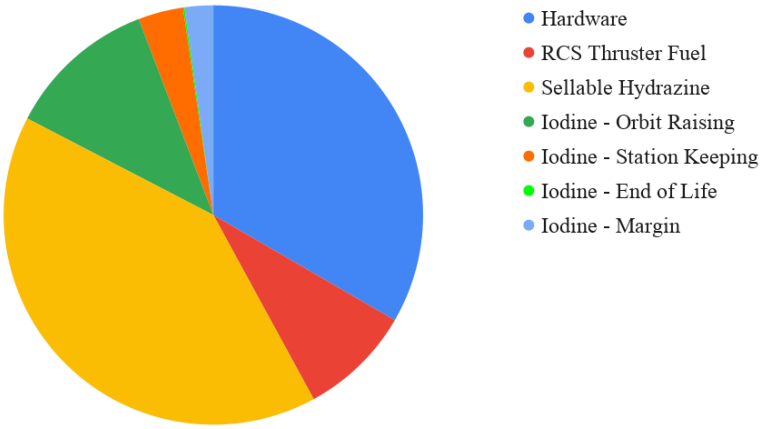

Fig. 7 Propulsion mass breakdown by category, totaling 17,455 kg.

B. Power Budget

The power budget, shown in Table 8, was derived from estimates of the two driving subsystems: propulsion and communications. The propulsion subsystem estimates were derived from the expected electric propulsion usage, consistent with the propulsion architecture described in Section 8.A. The communications subsystem estimate was calculated from a link budget consistent with the communications architecture described in Section 8.D. A 20% margin was applied to each subsystem estimate. Peak, nominal, and safe mode power values were determined for each of the driving subsystems, as shown in Table 8. The power usage of the other subsystems were deemed negligible.

Total solar panel area was derived using the method described in Section 21.2.2 of [7], based on the expected EOL power generation values of a 15-year lifetime. Triple-junction solar cells were assumed, with a power conversion efficiency of 22.3% and a yearly degradation rate of 0.5%. An inherent efficiency value of 88% was assumed to cover expected inefficiencies in the system. The total solar array area was found to be 61.0 m^2. The required battery size was derived using the method described in Section 21.2.3 of [7]. Assuming a 50% depth-of-discharge and a 98% efficiency, the total storage capacity required was calculated to be 39,000 W-hr. Ni-H_2 batteries were selected for the >15-year mission lifetime capability, as they offer demonstrated longevity and graceful degradation over extended missions. An energy density of 60 W-hr/kg was assumed. The resulting battery mass, distributed across at least 2 cells, is 650.0 kg.

Table 8 Power Budget Summary by Driving Subsystem

Subsystem		Peak Functionality (W)	Nominal Functions (W)	Safe Mode (W)
Communications	Total	227	157	63
	Minimum After Power Conditioning Loss (PCL)	254	179	71
	Target Power	305	211	85
Propulsion	Total	12,862	7,766	358
	Minimum After PCL	14,155	8,518	401
	Target Power	16,987	10,222	481
Full System Target Power		**17,292 W**	**10,433 W**	**566 W**

X. Environmental and Engineering Analyses

A. Thermal Analysis

1. Model Setup and Thermal Design

A thermal model of the MISO depot was developed in Thermal Desktop to evaluate on-orbit temperature distributions and heater sizing under pseudo-steady-state. The model comprises ~300 thermal nodes representing major structural and functional elements, including the propellant tankage, the cargo bay, structural panels, docking interfaces, the robotic arm, and communication electronics. The orbital environment was defined at 34,786 km altitude to calculate environmental heat loads from direct solar flux, Earth infrared emission, and Earth albedo. Optical and thermophysical material properties were sourced from [8, 9].

The thermal control strategy combines passive insulation, selective surface coatings, and active heater elements. All exterior except the +Z radiator is assumed to be covered in multi-layer insulation (MLI). The +Z face is coated with iridite aluminum (chromate conversion coat/Alodine/chem film) to provide a low absorptivity-to-emissivity ratio for heat rejection. Internally, the depot is divided into two thermally distinct chambers by a structural midplate. The lower chamber, housing the propellant tanks, uses iridite aluminum interior coatings to provide moderate radiative coupling while limiting thermal exchange with the MLI-wrapped tanks. The upper chamber is coated with black paint to promote radiative transfer from the midplate to the top plate, allowing waste heat to conduct upward and radiate through the +Z face. Communication components are mounted to the midplate so that their waste heat partially offsets iodine tank heater demand in the lower chamber.

Table 9 below shows the operational temperature limits (storage temperature limits for propellant tanks) for all temperature sensitive components. Active thermal control is limited to heaters on all propellant tanks. Heater set points were defined to maintain tank temperatures at least 10°C above these lower limits throughout the orbit.

Table 9 Temperature-Sensitive Component Operational Limits

Component	Min. Op. Temp. (°C)	Max. Op. Temp (°C)
Interface	-35	60
Hydrazine Tanks	10	40
Iodine Tanks	20	50
Battery (Ni-H_2)	-25	30

2. Results

The model was run over approximately 47.9 hours, corresponding to two full orbital periods, to capture cyclic environmental heating variation and evaluate temperature extremes and heater duty cycles. Results are summarized in Table 10 and Table 11 below.

Table 10 presents predicted temperatures and margins for all temperature-sensitive components. All components remain within allowable operational ranges with positive margins. The docking interfaces exhibit the largest cold-side margin at 52.0°C, reflecting favorable radiative coupling to the insulated spacecraft body. The hydrazine tanks, the most thermally constrained subsystem due to their narrow 10 to 40°C band, maintain a minimum cold-side margin of 10.4°C and a hot-side margin of 15.9°C, confirming that the combination of MLI and active heater control keeps propellant within its liquid operating range. The iodine tanks maintain a minimum margin of 11.1°C, and the nickel-hydrogen batteries remain well within limits with margins of 33.5°C and 20.7°C on the cold and hot sides, respectively.

Table 10 Component Temperature Predictions and Margins

Component	Min Margin (°C)	Min Temp (°C)	Max Temp (°C)	Max Margin (°C)
Interface	52	17	20.1	39.9
Hydrazine Tanks	10.4	20.4	24.1	15.9
Iodine Tanks	11.1	31.1	31.5	18.5
Battery (Ni-H_2)	33.5	8.5	9.3	20.7
Robotic Arm	-	8.3	9.2	-

Table 11 presents heater performance results. No heater power is required for the seven hydrazine tanks, as the MLI insulation, internal radiative environment, and waste heat from surrounding avionics maintain hydrazine well above its 10°C lower limit without active heating. All four iodine tanks, however, require continuous heating at 100% duty cycle, drawing an average of 15.0 to 16.2 W per tank and peaking at 20.9 to 22.2 W. Total average heater power for the iodine subsystem is approximately 62.7 W, with a recommended design allocation of 115.5 W to accommodate margin. This continuous demand is expected, as iodine must remain above its sublimation temperature and the high-altitude orbit produces long eclipse durations with minimal Earth infrared warming.

Table 11 Heater Resulting Power and Duty Cycles

Heater	Total Energy (J)	Average Power (W)	Duty Cycle (%)	Max Power (W)
Hydrazine 1 - 7	0	0	0	0
Iodine 1	2,713,530	15.7	100	21.7
Iodine 2	2,787,800	16.2	100	22.2
Iodine 3	2,577,250	15.0	100	20.9
Iodine 4	2,717,360	15.8	100	21.7
Total	**10,795,940**	**62.6**	**-**	**115.5**

B. Radiation Analysis

The depot will be orbiting near GEO, which lies in the Outer Van Allen belt. This exposes the depot to a high radiation environment that will damage electronics, sensors, and hardware if not shielded. Near GEO, relativistic electrons ranging from 0.1 to 10 MeV dominate the radiation environment along with solar particle events (SPEs) and galactic cosmic rays (GCRs). The total amount of radiation damage accumulated over time is called the total ionizing dose and heavily influences the amount of radiation shielding needed to protect electronics/components. An analysis using SPENVIS* was conducted to determine the sufficient shielding thicknesses required for electronics/components on board the depot.

1. Model Setup

The simulation was split into four phases to model the radiation environment the depot would experience throughout its entire operation: Low Earth Orbit (LEO) orbit (185 km), GTO transit and circularization (185 to 34,786 km), near GEO orbit (34,786 km), and EOL disposal. The radiation environment was then modeled in each phase using the NSSDC AP-8 and AE-8 models. The next section details the results of the simulation.

*The Space Enviroment Information System by ESA. Accessable: https://www.spenvis.oma.be/

2. Results

The plots in Figure 8 show the spectra of trapped protons and electrons that the depot will be exposed to throughout its mission duration. The results from the AP-8 model show that trapped protons are less prevalent than electrons, but have a larger range (0.1 to 400 MeV). These higher-energy protons (1 to 400 MeV), albeit in less quantity, come from SPEs and GCRs and cause damage to solar cells and electronics. The AE-8 model shows the prevalence of trapped electrons with the peak energy ranging between 0.04 and 2 MeV.

While electrons dominate the GEO environment in terms of flux, proton contributions often have a greater influence on shielding thickness due to their higher penetration capability. Aluminum is commonly used in aerospace applications to shield against these radiation effects. Figure 9 shows the radiation dosage over the entire mission duration as a function of aluminum shielding thickness. From this, it was determined that medium (3 to 6 mm) and thick (6 to 10 mm) spot shielding can be used to protect critical electronics and components based on their respective radiation ratings.

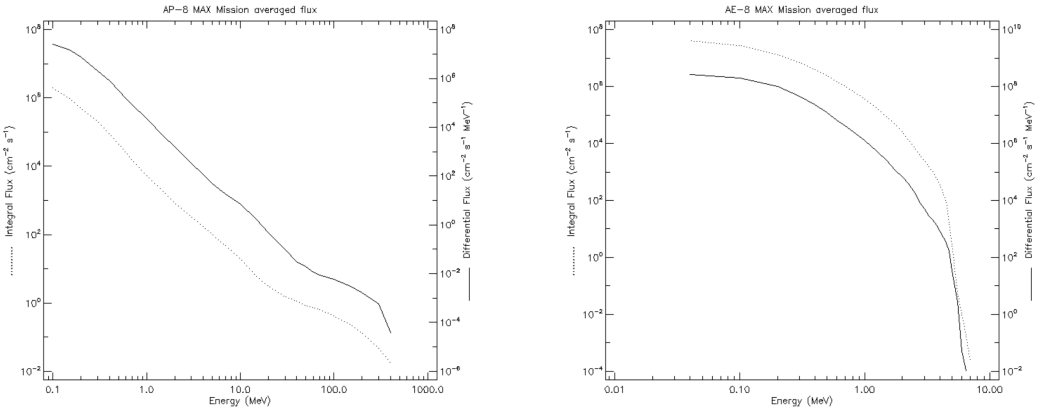

(a) (b)

Fig. 8 (a) Average spectra of trapped protons (b) Average spectra of trapped electrons

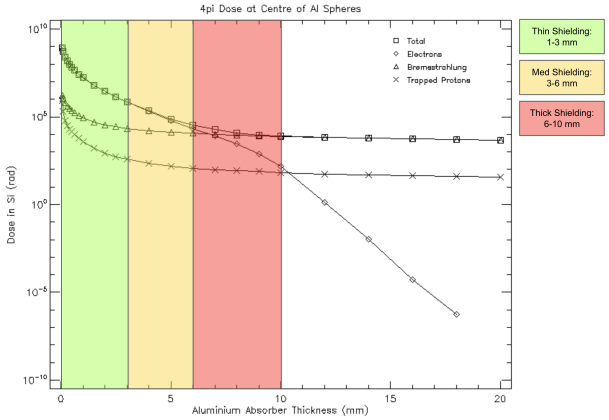

Fig. 9 Radiation dosage in Si as a function of aluminum shielding thickness (mm)

XI. Interfaces and Integration

A. Client Compatibility and Service Classes

Clients are grouped into three compatibility classes. Class A vehicles support docking, propellant transfer, and component handoff. Class B vehicles support docking and refueling only. Class C vehicles support docking and

hardware handoff but not propellant transfer. This classification aligns with current in-space servicing guidance, which emphasizes cooperative interfaces including fiducials, beacons, grapple fixtures, fluid transfer ports, and separable power and data interfaces to reduce operational risk. [1]

MISO's concept assumes compatibility across five servicing interface families rather than a single universal standard, reflecting the continued evolution of prepared servicing interfaces across multiple industrial implementations. Consequently, client compatibility must be established at the interface family level prior to mission planning, not during terminal operations. [1]

B. Keep-Out Zones and Proximity Operations Geometry

The current design shows a six-sided bus with overall dimensions of 3.51 m by 16.26 m by 3.57 m, six docking and fueling interfaces, and six deployable solar arrays. It also baselines five docking or refueling interfaces, a central cargo bay, and a 4.55 m robotic arm serving that bay. Approximating the bus as the regular hexagonal prism shown in the concept review gives a side-panel width of about 1.65 m per face. (Refer Figure 6a)

For docking-face design, that 1.65 m panel width is the controlling number. Using the current public International Docking System Standard (IDSS) geometry as a conservative reference envelope, the soft-capture petal base is about 1.20 m in diameter, the hard-capture guide-pin locating circle is about 1.375 m in diameter, and the transfer passageway is 0.80 m in diameter [10]. In other words, an IDSS-class prepared docking envelope would consume most of one MISO side panel by width. That makes adjacent-face simultaneous occupancy poor practice. A client on one face and a second client on the neighboring face would be separated by only 60° in azimuth, which is too tight once approach sensors, capture hardware, client appendages, and relative-attitude dispersions are included.

The ideal option for MISO is therefore one active docking corridor at a time, with any future concurrent occupancy limited to alternating faces that are 120° apart. The active approach corridor is tied to the selected docking face. However, it is also important to note that based on the client spacecraft's dimensions, it is also theoretically possible to host spacecrafts on all six sides. At the current moment, determining the ability or freedom of selecting this option is limited.

CONFERS prepared-capture guidance gives a useful starting template of a 10 km rendezvous sphere, a 1 km approach sphere, a 200 m keep-out sphere, hold points at 80 m, 15 m, and 1 m, and a final 10° conical approach corridor centered on the docking port [11]. For MISO, that means each side face that is opened for traffic needs its own protected 10° terminal cone normal to the panel, while all other faces remain closed to approach. Since the depot supports multiple interface families, the face assignment should be performed before rendezvous begins, before the client enters the 200 m zone.

Solar array keep-out geometry is the dominant geometric constraint for MISO. The baseline depot uses a six-sided bus with six deployable solar panels, and the fully deployed spacecraft envelope is 13.20 m across its largest dimension, with body dimensions of 3.57 m by 2.86 m. Accordingly, the solar-array exclusion region should be defined as the union of six panel deployment and articulation volumes around the hexagonal bus. During rendezvous and docking, these six panel envelopes bound the allowable approach geometry, since any client trajectory that crosses a panel deployment sector or the power-tracking sector would violate the depot keep-out zone. Operationally, this means docking should be constrained to a designated active port and the six arrays should be driven to a pre-qualified safe attitude before the client enters the final approach corridor.

C. Verification, Fault Containment, and Post-Service Validation

The integration architecture would gate every servicing phase with explicit verification. Before docking, MISO would validate client interface family, relative pose quality, approach corridor compliance, and keep-out clearance. After hard capture, it would verify latch state, structural settling, propellant-line integrity, and telemetry consistency before enabling any fluid path. After component handoff, it would verify seating, load release, visual alignment, and client-side acknowledgment before arm release and departure. This sequence is already reflected in the concept risk controls, which include dual isolation valves, leak-check sequencing, autonomous abort on abnormal pressure or flow, independent retreat logic when navigation uncertainty grows, and redundant confirmation sensing before arm release. IDSS places final docking analyses and hardware verification responsibility on the spacecraft developer. International External Robotic Interface Interoperability Standards, similarly states that interface verification should be performed through compatibility testing, integrated end-to-end testing, and system-level analysis. [10], [12] In summary, MISO's interface philosophy would remain deliberately constrained. The depot would service only prepared spacecraft whose external geometry, docking hardware, navigation aids, fluid path, and component installation points are declared in advance.

That constraint narrows the initial client pool, but it converts servicing from an exceptional proximity operation into a repeatable logistics transaction.

XII. Risk Assessment

A structured risk analysis was conducted to evaluate potential threats to mission success. Risks were assessed using a severity versus probability framework, with consideration given to detectability where applicable. Based on this assessment, high-priority risks were identified and mitigation strategies were developed to reduce both their likelihood and impact. Table 12 highlights the most significant risks to the MISO mission.

Table 12 Major and moderate mission risks and associated mitigation strategies.

Risk ID	Description and Mitigation
R-PROP-03	Propellant leak or contamination during refueling. Mitigation: Dual isolation valves; leak-check sequencing before transfer; inline filtration; autonomous abort capability.
R-RAD-02	Radiation-induced degradation of servicing components reduces operational reliability. Mitigation: Radiation-tolerant electronics and shielding; fault detection and reconfiguration capability after upsets.
R-SRVC-11	Verification of module transfer fails to detect unsuccessful handoff
R-STRC-04	Long-term material degradation from thermal cycling reduces structural strength

XIII. Future Work

This concept study establishes a baseline depot architecture and demonstrates its feasibility across the major subsystems. Several areas of future work would strengthen the design and advance the concept toward higher fidelity. The current baseline assumes a circular, equatorial sub-GEO orbit, but the trade space for eccentricity and inclination was not fully explored. Introducing non-zero eccentricity could provide periodic altitude variation that reduces launch mass requirements, lowering propellant costs and potentially allowing customers to purchase additional fuel to compensate for the higher Δv needed to reach an elliptical orbit while still achieving a net cost savings. Inclined orbits could extend the depot's market to customers operating in inclined constellations such as GPS in MEO. A multi-disciplinary optimization coupling Δv cost, propellant pricing, thermal loads, radiation exposure, ground station contact windows, servicing response time, and launch mass would enable a more rigorous selection of the operational orbit.

The current concept assumes a single depot serving client servicers that transit from GEO via Hohmann transfer. Deploying multiple depots distributed across different altitudes, inclinations, or phasing slots would reduce Δv and TOF burdens on individual clients. A multi-depot architecture introduces logistics coordination challenges (resupply transit times between depots, optimal distribution of propellant and component inventories across nodes, and scheduling of depot-to-depot transfers to balance utilization) that would benefit from simulation-based analysis to determine whether the infrastructure-level cost savings justify the added operational complexity. These two lines of investigation also open the possibility of exploring unconventional depot constellation geometries. One concept of interest is a set of depots in highly elliptical orbits with staggered phasing, where each depot periodically sweeps through both the LEO and GEO altitude bands, offering transient access windows at multiple regimes. Challenges including thermal cycling, radiation exposure variation, and communication link scheduling would need to be assessed.

Additionally, if the MISO system design were to progress, a detailed structural analysis effort would be required to verify compatibility with the launch environment of Falcon Heavy and ensure overall structural integrity. This would include development of a finite element model to evaluate stresses, deflections, and margins of safety under quasi-static launch loads, as well as a modal analysis to confirm that natural frequencies meet launch vehicle requirements. Additional analyses would address random vibration, acoustic loading, and shock events associated with stage separation and fairing deployment. Critical subsystems including the propellant tank supports, payload interfaces, and the stowed robotic arm would be assessed for survivability. These efforts would be complemented by a verification and testing plan aligned with established standards to ensure the design is fully qualified for flight.

XIV. Conclusion

In conclusion, MISO represents a step toward shifting space operations from disposable, single-use spacecraft to serviceable, scalable infrastructure. By demonstrating that a dual-function depot combining refueling and component logistics is technically and economically feasible, this work contributes to the foundational concept study for a sustainable in-space logistics network capable of supporting more ambitious and longer-duration missions.

Acknowledgments

The MISO team would like to thank our faculty advisor, Professor Aaron Johnson of the Aerospace Engineering depart at the University of Michigan for his oversight and support of this endeavor. We would also like to thank Dr. Ed Tate of Virtus Solis Space for his technical expertise and continuous mentorship of the team throughout the academic year. Without these two, the formation and success of the team would not have been possible.

References

[1] Mulvaney, J., Arney, D., and Williams, C., "In-Space Servicing, Assembly, and Manufacturing (ISAM) State of Play: 2025 Edition," NASA Technical Memorandum NASA/TM-20250008988, 2025. Available: https://ntrs.nasa.gov/citations/20250008988

[2] Sevigny, T., and Jia-Richards, O., "Orbital Optimization of Servicing Depots for Minimized Response Time in GEO," *2026 AIAA Region 3 Student Conference Proceedings* (not yet published)

[3] Skelton, E., and Velasquez, A. E., "Rendezvous Fiducial Implementation in a Space Vehicle Life Cycle," Proc. 46th Rocky Mountain AAS Guidance, Navigation, and Control Conf., Breckenridge, CO, Feb. 2024, NASA NTRS 20230018477.

[4] Jones, N., "Satellite servicing is taking off," Nature, Vol. 600, 2021. Available: https://www.nature.com/articles/d41586-021-03384-8

[5] Busek Co. Inc., "BHT-6000 Hall Effect Thruster," Product Datasheet, accessed 2026. Available: https://www.busek.com/bht6000

[6] Hofer, R. R., and Randolph, T. M., "Mass and Cost Model for Selecting Thruster Size in Electric Propulsion Systems," Proceedings of the 30th International Electric Propulsion Conference (IEPC-2007-287), Florence, Italy, 2007. Available: https://electricrocket.org/IEPC/IEPC-2007-287.pdf

[7] Wertz, J. R., Everett, D. F., and Puschell, J. J., *Space Mission Engineering: The New SMAD*, 1st ed., Microcosm Press, Hawthorne, CA, 2011. Available: https://www.scribd.com/document/387046605/James-Wertz-Space-Mission-Engineering-The-New-SMAD-2011

[8] Gilmore, D. G., "Appendix A: Surface Optical Property Data," Spacecraft Thermal Control Handboon, 2nd ed., Aerospace Press, 2002, pp. 791-801.

[9] Gilmore, D. G., "Appendix B: Material Thermal Properties," Spacecraft Thermal Control Handboon, 2nd ed., Aerospace Press, 2002, pp. 802-818.

[10] International Docking System Standard (IDSS) Committee, International Docking System Standard Interface Definition Document (IDSS IDD), Rev. G, M2M-30209, Jan. 23, 2026. https://internationaldeepspacestandards.com/wp-content/uploads/2026/01/M2M-IDSS-IDD-Rev-G-1-23-2026.pdf

[11] CONFERS, Recommendations for Best Practices, Functional Requirements, and Norms for Prepared Free-Flyer Capture and Release, Consortium for Execution of Rendezvous and Servicing Operations, 2022. Available: https://cdn.ymaws.com/satelliteconfers.org/resource/resmgr/confers_publications/confers_recommendations_for_.pdf

[12] International Deep Space Interoperability Standards, International External Robotic Interface (IERIIS) Robotic Baseline, Rev. 3, March 2019. Available: https://internationaldeepspacestandards.com/wp-content/uploads/2024/02/robotic_baseline_final_3-2019.pdf